Complex Denoising of MR Data Via Wavelet Analysis : Application for Functional MRI.

Saleem Zaroubi[1,2] and Gadi Goelman[1]

1- Human Biology Research Center
Department of Medical Biophysics and Nuclear Medicine
Hadassah Hebrew University Hospital
Jerusalem, Israel

2- Max Planck Institut für Astrophysik
Karl Schwarzschild Str. 1
65748 Garching bei München, Germany

Abstract

A fast post-processing method for noise reduction of MR images, termed complex-denoising, is presented. The method is based on shrinking noisy discrete wavelet transform coefficients via thresholding, and it can be used for any MRI data-set with no need for high power computers. Unlike previous wavelet application to MR images, the denoising algorithm is applied, separately, to the two orthogonal sets of the complex MR image. The norm of the combined data is used to construct the image. Using this method, signal-noise decoupling and Gaussian white noise assumptions used in the wavelet noise suppression scheme, are better fulfilled.

The performance of the method is tested by carrying out a qualitative and quantitative comparison of a single-average complex-denoised image of a standard phantom with a multiple averages images of the same phantom; and with a traditionally wavelet denoised, image obtained from the same data. The comparison shows that the complex-denoising scheme improves the signal--to-noise and contrast--to--noise ratios more than the traditional-denoising scheme. The main advantage of the complex-denoising methods is in low SNR regions, where in high SNR regions complex and traditional wavelet denoising methods are equivalent.

The method is applied to fMRI data. It is shown that the activation area in a cross-correlation analysis is 150% larger in the complex-denoised versus original data sets when equal threshold value is used. Using principal component analysis approach, the variance of the first few principal components is significantly bigger (by 70%) in the complex-denoised set compared with traditional-denoising or the original sets.

1. Introduction.

In the last few years several magnetic resonance imaging (MRI) techniques yielding information on human brain neuronal activity were introduced[1-10]. These techniques provide high spatial and temporal functional anatomy resolution, and allow longitudinal studies since some are completely non-invasive. The success of these functional MRI (fMRI) techniques to determine functional sites of various tasks, made fMRI a center tool in neuro-imaging. To increase temporal resolution, echo planar imaging (EPI) techniques are being used resulting in multiple slices images, in about a second. These images have low signal to noise ratio particularly where one need a better spatial resolution.

In this paper we present a nonlinear denoising algorithm based on wavelet analysis that suppress the Gaussian white noise. This method is a modification of a known denoising procedure that is especially suited to MRI data. It is shown that the modified wavelet denoising algorithm is superior to other wavelet denoising methods particularly, for low SNR images. Therefore, it specifically suited for fMRI data-sets. Recovery of an image from noisy MR data is a classic problem of inversion. A straight-forward inversion is often unstable and a regularization or some processing scheme is needed in order to interpolate where data are noisy. Image processing spans a variety of methods, starting from the classical, *e.g.,* Wiener filtering [11, 12] and Principal Component Analysis [13], to the more modern, and usually non-linear, such as Artificial Neural Networks [14], Maximum-Entropy [15], or Wavelets analysis[16-18]. All of these methods attempt, subject to some assumptions, to extract the maximum amount of `useful' information from the data.

In many of those methods the data are expanded in some functional basis that maintains their phase distribution as well as their power spread over various scales, *i.e.*, power spectrum. With a clever choice of functional basis, it is often possible to distinguish between the various contributions to the MR data and to filter the noise. In this paper we choose to work with a non-linear denoising scheme in Wavelet space, where Gaussian white noise is especially easy to pick out from the raw data [19-21].

During the last decade wavelets have become a popular tool in various data analysis and signal and image processing applications. Wavelet functional bases' main appeal stems from their simultaneous localization in both the wave-number (frequency) and the position (time) domains, where they allow for an orthogonal and complete projection on modes localized in both spaces, therefore make possible a multi-resolution analysis. The localization allows compressing the noiseless data features into a very small number of very large wavelet coefficients. Gaussian white noise, however, stays as white noise in any orthogonal basis, therefore spreading, in wavelet space, over all expansion coefficients and contribute to each of them a relatively small amplitude. Consequently, in wavelet basis, the noiseless signal dominated coefficients can be easily singled out from their noise dominated counterparts[19, 20, 22]. In summary, decomposition via wavelets has two main advantages: First, it maintains spatial (temporal) as well as characteristic wave-number (frequency) information. Second, many classes of functions can be expanded in relatively few number of wavelet basis functions while keeping most of their information content. These two properties make of wavelets an excellent tool for denoising and data compression[19, 23].

Application of wavelets for denoising of MR images has been pioneered by Weaver et.al.[24] who applied their denoising scheme on MR images of the human neck and concluded that the denoising scheme can reduce noise from 10 to 50% without reducing edge sharpness. Other than denoising via wavelets [24-27], researchers has found many other wavelet applications to MRI, including wavelet encoding of MR images (*e.g.,*[26, 28, 29]) and MR data compression (*e.g.,*[30]).

In the above application of wavelet denoising of MRI data, the denoising was performed on the images themselves. However, in MRI the image noise is not Gaussian. Rather, the Gaussian noise assumption is more correctly used to each component of the complex MR data separately. In this paper, Daubechies discrete wavelet basis [16] is utilized in order to suppress the noise from each of the complex MR data components, separately; the image is then reconstructed from the data components. In this way, the assumption of Gaussian white noise is employed for each of the data components. We show that by this way, one improves the SNR similarly to [24], however, at low SNR images our new approach performs better. Since fMRI data suffers usually from low SNR, the new denoising algorithm is especially suited for fMRI data. We show that activation areas obtained from fMRI complex denoised data have a higher correlation with the stimulus compared with the activation areas obtained from the original and absolute denoising data.

2. Denoising by Wavelets

MR image is viewed as a two dimensional set of $N \times N$ observations modeled mathematically, after Fourier transform, as

$$I^{obs} = I + \varepsilon \qquad [1]$$

where, $I = \left\{I_{x_i, y_i}\right\}$ is the underlying localized signal at position (x_i, y_i) and $\varepsilon = \left\{\varepsilon_{x_i, y_i}\right\}$ is the statistical uncertainty assumed to be Gaussian white noise. The first step in denoising the data is to transform them to wavelet space as $I^{obs}_{\alpha\beta}$ where α and β are two dimensional index vectors, each corresponding to wavelet's resolution and location along each dimension. Note that Gaussian white noise with standard deviation σ in real space stays as such in wavelet space due to the orthonormality and completeness of the discrete wavelet transform (DWT) functional basis.

To study the noise behavior, it is instructive to construct the data sorted wavelet spectrum (SWS), which is the amplitude list of the wavelet coefficients ranked in decreasing order. Typical behaviors of the noisy real, imaginary and absolute values of MR image are shown in Figure 1. Inspection of the log-log plot of the SWS of the real and imaginary parts of the data (solid lines in Figs 1B & 1C) reveals two distinct regions, the first consists of a modest decline in the high amplitude region of the spectrum, that breaks sharply into a lower amplitude region where the wavelet coefficients are dominated by the white noise. The break 'level' is in accordance with the standard deviation of the image background noise ~ 10^4. In other words one expects the break to approximately occurs at wavelets coefficients with SNR~1, namely, approximately at twice the standard deviation of the background noise, as indeed the case here.

Having identified the onset of noise dominated regime, one then attempts to obtain an unbiased noise-free estimator of the signal in the wavelet domain,

$$\hat{I}_{\alpha\beta} = \hat{I}_{\alpha\beta}\left(I_{\alpha\beta}^{obs}, \lambda\right) \qquad [2]$$

where λ is a pre-determined parameter. Donoho [31] and Donoho & Johnstone [20, 22] proposed the `soft' thresholding estimator

$$\hat{I}_{\alpha\beta} = sign\left(I_{\alpha\beta}^{obs}\right)\left(|\, I_{\alpha\beta}^{obs}\,| - \lambda\right)_{+} \qquad [3]$$

which `kills' noise prevalent coefficients and keeps, with $\lambda$ reduction, `true' signal dominated wavelet coefficients. The constancy of Gaussian white noise power spectrum over all resolution scales makes of the soft thresholding rule (Eq. [3]) an ideal estimator. Since the measurement modeling assumed in Eq. [1] and the normal white noise assumption hold in the real and imaginary parts of the data separately, one has to apply the denoising algorithm to each of them separately. For the image, defined to be the norm of the two data components, both assumptions are not valid. Due to the signal-noise coupling in the data absolute value, it is practically impossible to distinguish noise from signal dominated coefficients. This can be shown by considering a complex datum point $c = (a \pm \varepsilon_1) + i(b \pm \varepsilon_2)$ where $\varepsilon_1$and ε_2 are the errors in each component. The coupling terms in the datum absolute value,

$$|c| \approx \sqrt{a^2 + b^2 \pm 2a\varepsilon_1 \pm 2b\varepsilon_2 + \varepsilon_1^2 + \varepsilon_2^2} \qquad [4]$$

are obvious. This coupling is the main reason for applying the denoising scheme to each of the complex data components separately. In the examples shown in Figures 1B, 1C & 1D, the background noise level determines the value of $\lambda \approx 10^4$. Note however, that for very low SNR (<<1) Eq. 4 becomes

$$|\, c \,| \approx \sqrt{\varepsilon_1^2 + \varepsilon_2^2} \pm \frac{\varepsilon_1 a \pm \varepsilon_2 b}{\sqrt{\varepsilon_1^2 + \varepsilon_2^2}} \qquad [5]$$

where for a dominant noise term, say ε_1, the signal and noise decouple to give the relation $|c| \approx |\varepsilon_1 \pm a|$, which in turn accounts for the break seen in fig. 1D.

3. Demonstration on a phantom sample.

To test the denoising algorithm we apply it to MR data of a standard phantom sample. The phantom sample consists of a plastic structure filled with several solutions each with different relaxation time. The sample was put in a Bruker-Biospec 4.7T and a 20cm volume coil was used. MR images were acquired using the fast spin echo technique, with TR of 150ms, TEeff of 120ms and matrix size of 512x256 with 2mm slice width.

The MR raw image consists of two orthogonal components, presented as real and imaginary parts of a complex number. Commonly, noise in MR images is assumed to be Gaussian and not coupled with the signal (Eq. [1]), assumptions that hold for the real and imaginary components separately. Therefore, in order to exploit the thresholding algorithm to its fullest potential the denoising should be applied separately to each component after making sure that their phases are in order. Figures 1B & 1C show the sorted wavelet spectra of the real and imaginary components (solid lines). Each of these spectra consists of two distinct regions, corresponding to signal dominated coefficients (high amplitude) and noise dominated coefficients (low amplitude). Independent measurement of the standard deviation of the background, show that it coincides with about half the amplitude of the SWS break-down level (Figures 1B & C), which supports our denoising approach. The dashed lines in Figs. 1B-D depict the denoised SWS used to reconstruct the image in each case (see Fig. 2). These lines were calculated using the soft thresholding method with the threshold taken as the standard deviation of the background noise.

Figure 2 shows the various reconstructed images. The phantom sample raw image is shown in Fig. 2A. The reconstructed image, after denoising the real and the imaginary components separately, is shown in Fig. 2B. In this case, note the apparent improvement in SNR and contrast to noise ratio (CNR). The denoising method is applied to the absolute values of the raw data and the reconstructed image obtained is shown in Fig. 2C. In this case, there is an improvement in SNR, but the low SNR areas are not fully recovered. For comparison, a 4-averages image of the same phantom is shown (Fig. 2D).

In order to quantitative the comparison, we choose several regions of interest (ROIs) on the image (marked on the image attached to table 1), and calculate the mean and standard-deviation of those ROIs for each the raw, complex-denoised, absolute-denoised, 4-averages and 22-averages images. Table 1, shows very clearly the superiority of complex-denoising scheme over the absolute-denoising scheme, where the mean and standard-deviation of the former is closer to those of the 22-averages image in all ROIs. The complex-denoised performs better than the 4-averages image in all ROIs in terms of standard-deviation, and two of the ROIs (those with low SNR) in terms of mean. These results show the large improvement in SNR, about a factor of 2, obtained with the complex-denoising scheme.

4. Application to fMRI.

4.1. Method

To demonstrate the strength of the method in fMRI, we applied the denoising method to fMRI data of somatosensory stimulation applied on rats. The data was acquired as follows[32]: Male Sprague-Dawley rats (250-350 gr) were anesthetized with urethane i.p. (150mg/100gr) and put in a Bruker-Biospec 4.7T. The rats' heads were secured in a home built head holder, body temperature was measured with a rectal thermometer and kept constant by a feedback water blanket. A pair of small needle-electrodes were inserted under the skin of the right or the left hindlimb. The stimulation consisted of 0.3ms rectangular pulses with frequency of 3Hz and amplitude between 10 to 25 volts. A 20mm diameter surface coil was used to transmit rf pulses and receive the signal. The surface coil was placed over the skull and centered over the midline of the animal. Coronal slices positioned between bregma 0.5 and -2.5 were taken. MR images were acquired using the gradient echo (GE) sequence (TE=40ms, TR=80ms) with field of view of 2.56cm, 1mm slice thickness and resolution of 64x64. The flip angle was ~35^{o} in the cortex and lower in deeper structures. Non-periodic 8th order Hadamard matrix rows were used for stimulation in order to avoid any harmony with physiological fluctuations. Two non-periodic rows [-++-+--+]and [-+-++-+-] were used with '+' indicating stimulation on and '-' indicating stimulation off. In each time segment, 10 images were collected (51.2sec) such that each data set contained 80 images and lasted 6.82min. An interval of at least 15min was used between successive experiments.

4.2. Data analysis

Image analysis was performed in an external computer using IDL (Interactive Data Language). Two different statistical approaches were used to examine the difference between the complex denoised, absolute-denoised and the original data-sets. 1). Cross correlation analysis: Each pixel in the data-sets was cross correlated with the stimulus time course function and a correlation map was performed. A threshold of C=0.4, corresponding to $p<0.0001$, was used in these maps. The number of pixels above the threshold was calculated and compared. In the comparison we assumed that higher number presents better correlation with the stimulus. 2). Principal component analysis (PCA)[32]: PCA was performed on the data-sets and the variance of the top three components were compared.

4.3. Results

Figure 3 shows the potency of the denoising algorithm when used with fMRI data. Four images, chosen arbitrarily, from one of the fMRI data-sets are shown. Each image is shown after subtracting the mean of the 80 images. The subtraction is imperative as we are interested in relative changes in the images of the sequence. Note the low SNR of the subtracted images, this SNR makes the new denoising algorithm so efficient. The lower raw in Fig.3 shows the raw images, the second shows the complex-denoised images and the upper raw shows the absolute-denoised images. The improvement introduced to images after both complex-denoising and absolute denoising schemes is evident. It obvious also that the contrast to noise ratio (CNR) and SNR is superior in the complex-denoised fMRI data.

In figure 4 we show an example of the difference in the principal components and cross-correlation maps obtained with undenoised (original), complex-denoised and absolute denoised data-sets. The variance of the first principal component (PC) in the complex-denoised set is about twice the variance of the corresponding PC in the original set (11.3% vs. 6.5%) while is little better than the variance of the corresponding PC in the absolute denoising set (10.6%). The other PCs exhibit a similar relation. Using cross-correlation analysis we obtain similar pattern: The activation areas (correlation above 0.4) is larger in the complex-denoising set(398 pixels), reduces its size in the absolute denoising set (350 pixels) and quite small in the original set (190 pixels). This is a direct consequence of the SNR improvement in the denoised data-sets. Another case is presented in figure 5. In this figure we demonstrate that the PCs of the original and denoised sets have similar pattern with the PC of the denoised set of higher amplitude

The variance in the PCs and the number of pixels above threshold in the cross-correlation maps, in the original and the complex denoised sets were calculated in seven different fMRI data-sets. On average, we obtain an increase of 150% (!) in the activation area in the cross-correlation test, and an average increase of 70% in the variance of the first two PCs and an increase of 53% in the third PC, in the PCA test. This significant improvement justify the use of complex wavelet denoising in any fMRI data.

5. Conclusion

In this study we have presented a fast wavelet denoising method for improving MRI quality. The main new idea of this method is that it is applied separately to the two orthogonal components of the MR data. In this way, the basic assumptions used in the denoising algorithm, are better satisfied. The difference between the new and traditional wavelet denoising methods, is in low SNR images. It is shown that in these cases, the new method suppress the noise better without deteriorate image quality. An application of this method to a standard phantom sample shows a significant improvement in SNR and CNR. This improvement surpasses those achieved by the conventional wavelet denoising and other noise suppression methods, and does not require an extensive computational efforts.

The strength of the method is demonstrated with fMRI data-set. It was shown that the activation area, defined as the area in which the cross-correlation with the stimulus coefficient is above a chosen threshold, is larger in the complex-denoised sets compared with the absolute-denoised and original data-sets. This implies that for the same activation area, the average correlation coefficient in the complex denoised set, is higher then those obtain for the absolute wavelet denoising or the original sets. On average (n=7), the activation area was increased by 150%. Application of PCA resulted with similar conclusion. On average, the variance of the first three principal components have increased in the complex-denoised set over the original set by 70%,70%, and 53% respectively.

Thanks to the new method's computational efficiency, it can be used to reduce noise, even further, in a 3-dimensional (3D) data sets, where the algorithm is applied to the 3D data set as a whole. It is anticipated that a direct 3D denoising will significantly improve the outcome quality. This is particularly important in fMRI where multiple slices, to cover a large volume of the brain, is routinely acquired, either directly by echo planar volume or indirectly by multiple EPI slices.

In summary, it was shown that application of complex wavelet denoising on MR data result with significant improvement in image quality without penalty. The advantage of using this method was shown to be very significant in fMRI.

6. Acknowledgments

We would like to thank Drs. Y. Hoffman and N. Freedman for their comments on the manuscript. S. Z. would like to thank Dr. Y. Hoffman for introducing him to the world of wavelets. This work was supported by RASHI foundation, US-Israel Bi-national Science foundation grant # 95/40 (G.G.) and Israel Ministry of Science grant # 7699-1-95 (G.G.)

Reference

1. J.J. Neil, *The validation of freely diffusible tracer methds with nuclear magnetic resonance detection for measurement of blood flow.* Magn. Reson. Med., 1991. **19**: p. 299-304.

2. J.J. Ackerman, C. EWY, N. Becker, and R. Shalwitz, *Deuterium nuclear magnetic resonance measurements of blood flow and tissue perfusion employing 2H2O as a freely diffusible tracer.* Proc. Natl. Acad. Sci., 1987. **84**: p. 4099-4102.

3. J.W. Belliveau, B.R. Rosen, H.L. Kantor, R.R. Rzedzian, D.N. Kennedy, R.C. McKinstry, J.M. Vevea, M.S. Cohen, I.L. Pykett, and T.J. Brady, *Functional cerebral imaging by susceptibility-contrast NMR. Magn. Reson. Med.*, 1990. **14**: p. 538.

4. J.A. Detre, V.H. Subramanian, M.D. Mitchell, D.S. Smith, A. Kobayashi, A. Zaman, and J.S. Leigh, *Measurement of regional cerebral blood flow in cat brain using intracarotid 2H2O and 2H NMR imaging.* Mag. Reson. Med., 1990. **14**: p. 389-395.

5. B.R. Rosen, J.W. Belliveau, and D. Chien, *Perfusion imaging by nuclear magnetic resonance.* Magn. Reson. Q, 1989. **5**: p. 263-281.

6. J.A. Detre, J.S. Leigh, D.S. Williams, and A.P. Koretsky, *Perfussion imaging.* Magn. Reson. Med., 1992. **23**: p. 37-45.

7. R.R. Edelman, H.P. Mattle, and D.J. Atkinson, *Cerebral blood flow: assessment with dynamic contrast-enhanced T2*-weighted MR imaging at 1.5 T.* Radiology, 1990. **176**: p. 211-220.

8. J.W. Belliveau, D.N. Kenney, R.B. Buchbinder, R.M. Weisskof, M.S. Cohen, J.M. Vevea, T.J. Brady, and B.R. Rosen, *Functional mapping of the human visual cortex by magnetic resonance imaging.* Science, 1991. **254**: p. 716.

9. S. Ogawa, T.M. Lee, A.R. Kay, and D.W. Tank, *Brain magnetic resonance imaging with contrast dependent on blood oxygenation.* Natl Acad Sci USA, 1990. **87**: p. 9868-9872.

10. K.K. Kwonk, J.W. Belliveau, D.A. Chester, I.E. Goldberg, R.M. Weisskoff, B.P. Poncelet, D.N. Kennedy, B.E. Hoppe, M.S. Cohen, and R. Turner, *Dynamic magnetic resonance imaging of human brain activity during primary sensory stimulation. Proc. Natl. Acad. Sci (USA)*, 1992. **89**: p. 5675.

11. N. Wiener, *Extrapolation and Smoothing of Stationary Time Series*. Wiley, 1949, New York: .

12. S. Zaroubi, Y. Hoffman, K.B. Fisher, and O. Lahav, *Wiener reconstraction of the large scale structure.* Astrophysical Journal, 1995. **449**: p. 446-459.

13. I.T. Jolliffe, *Principal Component Analysis*. 1986, New York: Springer-Verlag.

14. J. Hertz, A. Krogh, and R.G. Palmer, *Introduction to the Theory of Neural Computation*. 1989, Redwood City, California: Addison-Wesley.

15. S.F. Gull, *Maximum Entropy and Bayesian Methods*. ed. J. Skilling. 1989, Kluwer. 53.

16. I. Daubechies, *Orthonormal basis of compactly supported wavelets.* Comm. Pure Appl. Math., 1988. **41**: p. 909-996.

17. I. Daubechies. *Ten lectures on Wavelets*. in *CBMS-NSF Regional Conference Series in Applied Mathematics*. 1992. Philadelphia, PA:

18. Y. Meyer, *Wavelets: Algorithms and Applications*. 1993, Philadelphia, PA: SIAM.

19. S.G. Mallat, *A theory for multiresolution signal decomposition: the wavelet representation.* IEEE Transaction on Pattern Analysis and Machine Intelligence, 1989. **11**(7): p. 674-693.

20. D.L. Donoho and I.M. Johnstone, *Ideal spatial adaptation via wavelet shrinkage.* Biometrika, 1994. **81**: p. 425-455.

21. D.L. Donoho and I.M. Johnstone, *Adapting to unknown smoothness via wavelet shrinkage.* J. Amer. Statist. Assoc., 1996. .

22. D.L. Donoho and I.M. Johnstone, *Adapting to unknown smoothness via wavelet shrinkage.* J. Amer. Statist. Assoc., 1994. .

23. J.M. Shapiro, *Embedded image coding using zero-trees of wavelet coefficients.* IEEE Transactions on Information theory, 1992. **38**: p. 617-643.

24. J.B. Weaver, Y. Xu, D.M. Healy, and L.D. Cromwell, *Filtering Noise from Images with Wavelet Transforms.* Magn. Reson. Med., 1991. **21**: p. 288-295.

25. J. Lu, J.B. Weaver, D.M. Healy, and Y. xu. *Noise Reduction with Multiscale Edge Representation and Perceptual Criteria*. in *Proc. IEEE-SP International Symposium on Time-Frequency and Time-Scale Analysis*. 1992. Victoria, BC:

26. D.M. Healy, J. Lu, and J.B. Weaver, *Two Applications of Wavelets and Related Techniques in Medical Imaging.* Annals. of Biomedical Engineering, 1995. **23**: p. 637.

27. M. Hilton, T. Ogden, D. Hattery, G. Eden, and B. Jawerth, *Wavelet denoising in functional MRI data,* in *Wavelet Application in Biology and medicine,* A. Aldroubi and M. Unser, Editors. 1996, CRC Press:

28. J.B. Weaver, Y. Xu, D.M. Healy, and J.R. Driscoll, *Wavelet-encoded MR imaging.* Magn. Reson. Med., 1992. **24**: p. 265-278.

29. L.P. Panych and F.A. Jolesz, *A dynamically adaptive imaging algorithm for wavelet-encoded MRI.* Magn. Reson. Med., 1994. **32**: p. 738-748.

30. A.A. Maldjian, W.C. Liu, D. Hirschorn, R. Murthy, and W. Semanczuk, *Wavelet transform based image compression for transmission of MR data.* AJR Am. J. Roentgenol., 1997. **169**(1): p. 23-26.

31. D.L. Donoho, *De-noising via soft thresholding*1992, Dept. of Statistics, Stanford University: Stanford.

32. G. Goelman and S. Zaroubi, *Observation of Two Distinct Modes of Activation in Somatosensory Stimulation: Functional MRI study via a combination of Principal Component Analysis and Cross-Correlation.* Magn. Reson. Med., **Submitted**.

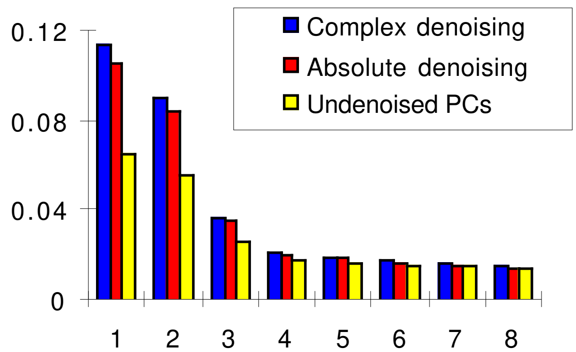
0.12
0.08
0.04
0
1
2
3
4
5
6
7
8
Complex denoising
Absolute denoising
Undenoised PCs

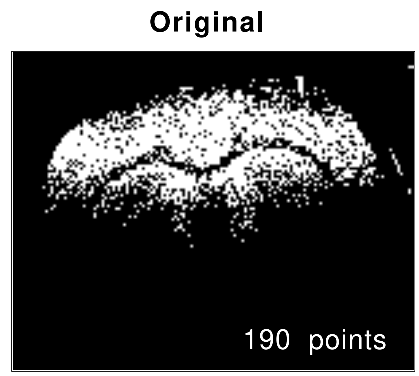
Original
190 points

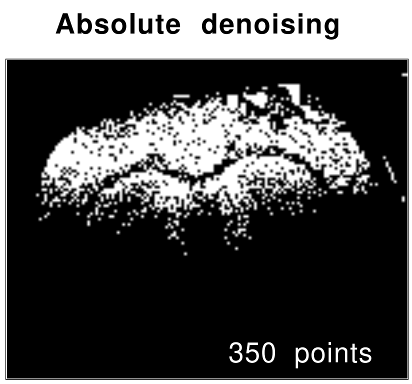
Absolute denoising
350 points

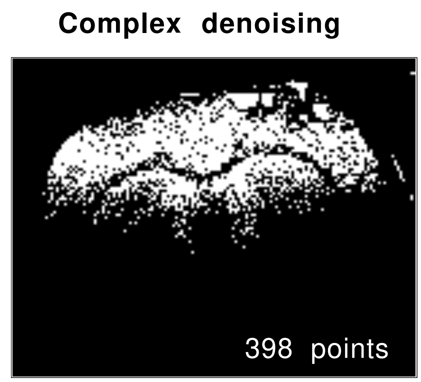
Complex denoising
398 points

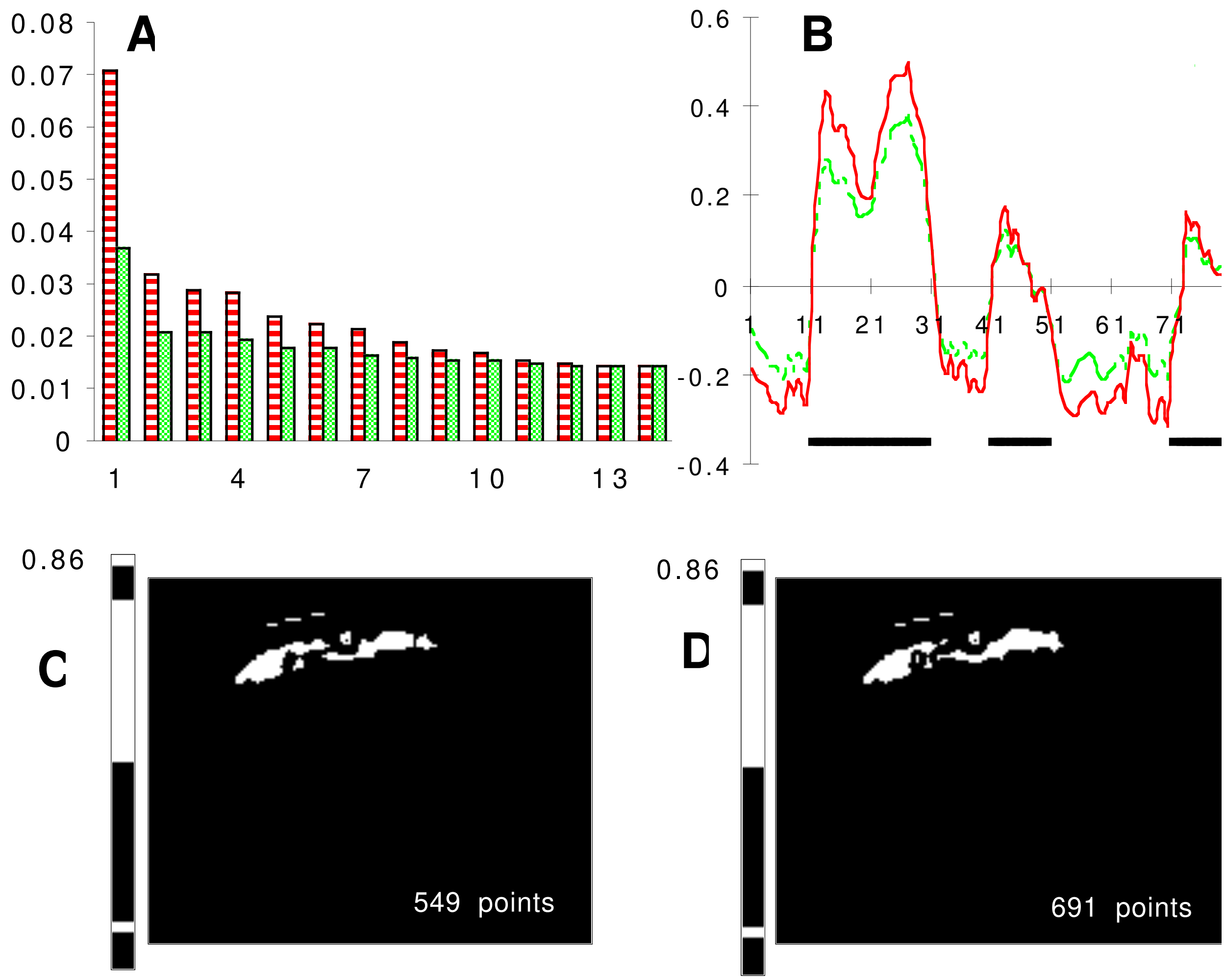
A
0.08
0.07
0.06
0.05
0.04
0.03
0.02
0.01
0
1
4
7
10
13
B
0.6
0.4
0.2
0
-0.2
-0.4
1
11
21
31
41
51
61
71
0.86
C
549 points
0.86
D
691 points